RSC Advances

PAPER

View Article Online
View Journal | View Issue

Cite this: *RSC Adv.*, 2017, **7**, 30807

Topological relations and piezoelectric responses of crystal-axis-oriented $BaTiO_3/CaTiO_3$ nanocomposites†

Dengwei Hu, *[a] Xiaomei Niu,[a] Hao Ma,[b] Wenxiong Zhang,[b] Galhenage A. Sewvandi,[c] Desuo Yang,[a] Xiaoling Wang,[a] Hongshei Wang,[a] Xingang Kong[d] and Qi Feng *[b]

2D crystal-axis-oriented mesocrystalline $BaTiO_3/CaTiO_3$ (BT/CT) nanocomposites with high-density heteroepitaxial interfaces were synthesized by a two-step solvothermal soft chemical process. The nanostructures, formation mechanism, topological relations between the BT and CT, and piezoelectric responses of the nanocomposites were investigated. The mesocrystalline nanocomposites are polycrystals constructed from crystal-axis-oriented BT and CT nanocrystals with the same crystal-axis orientation, respectively. The directions of the [001] and [1−10] of crystalline BT correspond to the directions of the [0−10] and [100] of crystalline CT, respectively. The mesocrystalline nanocomposites were formed *via* an *in situ* topochemical mesocrystal conversion mechanism. The density of the artificial BT/CT heteroepitaxial interface in these mesocrystalline nanocomposites can be adjusted by regulating the fraction of BT and CT in the nanocomposites. The mesocrystalline BT/CT nanocomposite with the composition close to BT/CT = 1/1 presents a large piezoelectric response owing to the lattice strain derived from its heteroepitaxial interfaces with the high density in the nanocomposite.

Received 3rd April 2017
Accepted 7th June 2017

DOI: 10.1039/c7ra03828c

rsc.li/rsc-advances

1 Introduction

Advances in atomic-level control of the heteroepitaxial nanostructures of functional nanocomposite materials have focused on the enhancement of the electrical properties of multicomponent metal oxide perovskites.[1–4] A lattice strain in such perovskites can effectively produce a high strain energy derived from the lattice mismatch sustained at their heteroepitaxial interfaces.[1,3,5,6] The high-density lattice strain at the heteroepitaxial interfaces is very beneficial for a large enhancement in the electrical properties.[3,7,8] Among the studies on nanocomposite perovskites with heteroepitaxial interfaces, $BaTiO_3/SrTiO_3$ (BT/ST) and $BiFeO_3$-based nanomaterials have been developed mainly by molecular beam epitaxy (MBE) and electrochemical deposition processes.[2–4,9,10] But these fabrication processes are complicated and expensive stacking configurations.[11,12] Therefore, the design of a new process to develop nanostructures with high-density heteroepitaxial interfaces is highly anticipated. However, nanostructures with high-density heteroepitaxial interfaces are difficult to obtain by traditional methods.

Mesocrystal is a polycrystal constructed from crystal-axis-oriented nanocrystals,[13] in which each oriented nanocrystal presents the same orientation direction. The electron diffraction pattern of a mesocrystal shows spots corresponding to the reciprocal lattice points as a single crystal.[14] It not only has properties based on the individual nanocrystal, but also exhibits unique collective properties and advanced tunable functions.[15,16] It can offer unique new opportunities for materials design.[13,17] Some 2D titanate mesocrystals were developed by our previous works.[18–22] Recently, we have reported that a mesocrystalline BT/ST nanocomposite with a mole ratio of Ba/Sr = 1 shows a remarkable enhancement of piezoelectric response by the BT/ST heteroepitaxial interface in the nanocomposite.[23] In the mesocrystalline BT/ST nanocomposite, tetragonal BT is a ferroelectric phase and cubic ST is a paraelectric phase. Although the $CaTiO_3$ (CT) and ST are alkaline earth metal titanates, there are some obvious lattice differences

[a]*College of Chemistry and Chemical Engineering, Engineering Research Center of Advanced Ferroelectric Functional Materials, Key Laboratory of Phytochemistry of Shaanxi Province, Baoji University of Arts and Sciences, 1 Hi-Tech Avenue, Baoji, Shaanxi, 721013 P. R. China. E-mail: hdwpolymer@yahoo.co.jp; Fax: +86-917-356-6366; Tel: +86-917-356-6589*

[b]*Department of Advanced Materials Science, Faculty of Engineering, Kagawa University, 2217-20 Hayashi-cho, Takamatsu-shi, 761-0396 Japan. E-mail: feng@eng.kagawa-u.ac.jp; Fax: +81-87-864-2438; Tel: +81-87-864-2402*

[c]*Department of Materials Science and Engineering, Faculty of Engineering, University of Moratuwa, Katubedda, Sri Lanka*

[d]*School of Materials Science and Engineering, Shaanxi University of Science and Technology, Weiyang, Xi'an, Shaanxi, 710021 P. R. China*

† Electronic supplementary information (ESI) available: Detailed experimental strategy, powder XRD patterns, SEM images, EDS-mapping TEM images, piezoelectric response of some materials reported, and Table S1 listing the atom mole ratios of Ti/Ba/Ca from corresponding EDS spectra. See DOI: 10.1039/c7ra03828c

between them. The artificial construction of lattice strain from the heteroepitaxial interface between these titanates can be realized. Therefore, the replacement of cubic ST by using orthorhombic CT is a new challenge and may be an effective method for the further enhancement of piezoelectric response.

In this report, we present a two-step solvothermal soft chemical process to synthesize 2D crystal-axis-oriented mesocrystalline $BaTiO_3/CaTiO_3$ (BT/CT) nanocomposites with artificial heteroepitaxial interfaces for the first time. The obtained 2D mesocrystalline BT/CT nanocomposites are polycrystals constructed from well-aligned BT and CT nanocrystals with the same orientation direction. Such 2D mesocrystal is very difficult to be obtained *via* the conventional self-assembly approach owing to their high orientation, high aspect ratio of two-dimension, and the chemical composition of two components. The topological relations between the crystal-axis-oriented BT and CT nanocrystals were investigated. The correlation between the piezoelectric response of and composition for the mesocrystalline nanocomposites has been revealed. Our findings imply a possibility of the simultaneous applications of the orientation engineering and the strain engineering to approach a huge piezoelectric response effect by using the characteristics of the mesocrystalline materials.

2 Experimental section

Sample preparation

All reagents used in this study were of analytical grade and without further purification. 2D single crystal precursors (thickness $\sim$ 200 nm) of $H_{4x/3}Ti_{2-x/3}\square_{x/3}O_4\cdot nH_2O$ ($\square$: vacancy of Ti, $x = 0.8$, $n = 1$, abbreviated as HT) with layered lepidocrocite structure were prepared as reported in our previous study.[24] Anatase TiO_2 nanoparticles (6.9 g), 5.1 g of KOH, 0.6 g of $LiOH\cdot H_2O$, and 25 mL of distilled water were sealed into a Hastelloy-C-lined vessel with internal volume of 45 mL and then heated at 250 °C for 24 h under stirring conditions. After the hydrothermal treatment, the obtained sample was washed with distilled water and dried at room temperature to obtain $K_{0.80}Ti_{1.73}Li_{0.27}O_4\cdot xH_2O$ (KTLO) crystals. The KTLO crystals (10.0 g) were treated with a 0.2 mol L^{-1} HNO_3 solution (1 L) for 24 h under stirring conditions to exchange K^+ and Li^+ in the layered structure with H^+, and then the sample was washed with distilled water. After the acid treatments were done twice, the layered protonated titanate HT single crystals were obtained. The as-obtained crystals were collected and washed with distilled water and alcohol, before air-drying at 60 °C for 6 h, and then the HT (6.2 g) single crystal precursors were obtained.

For the synthesis of the platelike crystal-axis-oriented mesocrystalline $BaTiO_3/CaTiO_3$ (BT/CT) nanocomposite, one-step solvothermal process was firstly tried by solvothermal treatments of HT (0.096 g)-$Ba(OH)_2$–$Ca(OH)_2$ mixture with different molar ratios of Ti/Ba/Ca in 30 mL solution using a sealed stainless-steel vessel with inner volume of 75 mL under different conditions. The pure BT/CT mixed phases cannot be obtained but some mixtures (see the ESI:† (1) one-step solvothermal soft chemical process). Therefore, we designed a two-step solvothermal soft chemical process for the preparation of the BT/CT nanocomposites. This process is gentle to keep the morphology of the starting matrix and is conducive to topochemical conversion reaction. In the first step, the HT precursors (0.096 g) were reacted partially with 30 mL $Ba(OH)_2$ solutions (mole ratio of Ti/Ba = 4 : 1, 2 : 1, 3 : 2, and 7 : 6, respectively) in a Teflon-lined, sealed stainless-steel vessel with inner volume of 75 mL at 200 °C for 12 h, to obtain the $BaTiO_3$/HT (BT/HT-1/3, -1/1, -2/1, -6/1) nanocomposites. The 2D homogeneous BT/HT nanocomposites generated in the water solvent were employed as precursors in the next step. In the second step, the generated homogeneous BT/HT nanocomposites were solvothermally treated at 200 °C for 12 h in 30 mL $Ca(OH)_2$ suspensions with the different concentration. A water–ethanol mixed solvent with a volume ratio of 5 : 25 was employed for the dispersion of the $Ca(OH)_2$ in the second step. To drive the reaction to completion, it is necessary that the excess 50% of Ca was placed in the reaction system. After the solvothermal treatment, the obtained sample was sequentially washed with the 0.2 mol L^{-1} acetic acid solution, distillated water, and ethanol. Finally, the obtained sample was dried at 60 °C for 12 h. The samples generated in the second step were designated as BT/CT-*x*/*y*, where *x*/*y* is a mole ratio of Ba/Ca. Therefore, the samples of the BT/CT-1/3, BT/CT-1/1, BT/CT-2/1, and BT/CT-6/1 were prepared from BT/HT-1/3, -1/1, -2/1, -6/1 samples, respectively.

For comparison purposes, the pure BT and CT mesocrystals without any heteroepitaxial interfaces were respectively prepared in pure water solvent from the HT precursor at 200 °C for 12 h *via* the solvothermal soft chemical process as reported by us previously also.[18,20] Although the platelike CT mesocrystals cannot be easily formed completely in this process,[20] a small number of CT mesocrystals with platelike morphology can be selected out easily and contrasted to the other titanates in this study.

Physical analysis

The structures of the crystalline samples were investigated using a powder X-ray diffractometer (XRD) (Shimadzu, XRD-6100; Rigaku, D/max-Ultima IV) with Cu Kα ($\lambda = 0.15418$ nm) radiation. The size and morphology of the crystalline samples were observed using scanning electron microscopy (SEM) (JEOL, JSM-5500S) or field emission scanning electron microscopy (FESEM) (Hitachi, S-900) or environment scanning electron microscopy (ESEM) (FEI, Quanta 250 FEG). Transmission electron microscopy (TEM)/(high-resolution TEM (HRTEM)) observation and selected-area electron diffraction (SAED) were performed on a JEOL Model JEM-3010 system at 300 kV, and the crystalline samples were supported on a Cu microgrid. Energy-dispersive spectroscopy (EDS; JEOL JED-2300T) was measured on the TEM system. Energy dispersive spectroscopy mapping (EDS-mapping) was observed using a combined HRTEM-EDS system (JEOL Model JEM-2100F HRTEM/EX-24063JGT EDX) as a function of the local relative concentration of the elements present.

Piezoelectric responses were measured by a scanning probe microscopy (SPM) system on a combined atomic force

microscope (AFM) and piezoresponse force microscopy (PRM) systems (SII, NanoTechnology Inc., Nano Navi Station; Bruker, Dimension Icon) with an SPA-400 probe. Silicon micro cantilever (SI-DF3-R, R: Rh precoated, $f = 28$ kHz, $c = 42$ N m^{-1}) and SiO_2/Si substrate were coated with an approximate 20 nm Au thin film by ion sputtering. The samples were dispersed on the Au thin film by drop casting. The location of an individual mesocrystal was detected by the conductive AFM probe tip with a conductive Au-coated Rh-precoated Si cantilever in the contact mode. After that a bias from −10 to 10 V was applied to the surface of the mesocrystal, and the information of the strains of the mesocrystal was gathered at the same time and detected from the global deflection signal using a built-in lock-in amplifier connected to the AFM. The effective piezoelectric coefficient d_{33}^* value was calculated by the formula

$$d_{33}^* = \frac{DV_{pr}}{V_{ac}} = \frac{\Delta l}{V_{ac}} = \frac{S}{V_{ac}}$$

where D is the AFM detector sensitivity, V_{pr} is the rms amplitude of the tip deflection voltage, V_{ac} is the rms amplitude of the applied voltage, Δl is the root-mean-square (rms) amplitude of the tip deflection, and S is the strain. Details of the measurement procedure and parameters can be found elsewhere.[23,25,26]

3 Results and discussions

Characterization of samples

XRD patterns of samples. Fig. 1 shows the XRD patterns of the samples obtained in the second step. It is very interesting that the strong diffraction intensities for BT and CT (ICDD file no. 42-0423, orthorhombic) phases can be simultaneously observed (Fig. 1b and c), when the mole ratios of Ba/Ca are 1/1 and 2/1, respectively. Although the crystal structure of BT is tetragonal at room temperature, the diffraction lines of BT obtained in this study are indexed based on the pseudocubic unit cell because of small tetragonal distortion and can be identified by ICDD file no. 74-1964 (cubic symmetry).[27] When the mole ratios of Ba/Ca are 1 : 3 and 6 : 1, respectively, the diffraction intensities of CT and BT phases present a very strong contrast (Fig. 1a and d); namely, one is strong and another is feeble. When the mole ratios of Ba/Ca is 1 : 1 and the pure ethanol was employed as the reaction solvent, pure BT/CT mixed phases cannot be obtained but a complicated mixture including anatase (ICDD file no. 21-1272), abundant BT, trace amounts of CT, unreacted HT and $Ca(OH)_2$ (ICDD file no. 84-1272) (Fig. 1e). These results imply that the pure BT/CT mixed phases can be obtained by the solvothermal treatment of the homogeneous BT/HT nanocomposites in the water–ethanol mixed solvent. The composition of BT and CT in the mixtures can be controlled by the instruction of BT contents.

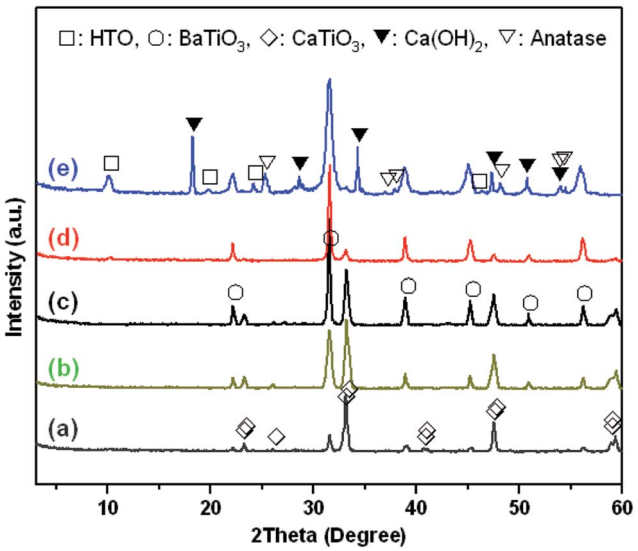

Fig. 1 XRD patterns of samples of (a) BT/CT-1/3, (b and e) BT/CT-1/1, (c) BT/CT-2/1, and (d) BT/CT-6/1 obtained by solvothermal treatments of different BT/HT nanocomposites and $Ca(OH)_2$ in (a–d) water–ethanol mixed solvent with volume ratio of 5 : 25 and (e) pure ethanol solvent at 200 °C for 12 h, respectively.

FESEM images of samples. The size and morphology of the crystalline samples were observed using SEM (see Fig. S3 and (2) two-step solvothermal soft chemical process in the ESI†) and FESEM (Fig. 2). All the obtained BT/CT-x/y samples present a typical irregularly platelike morphology. The thickness of the platelike particles is approximate 210 nm, and these platelike particles show a size of 2–5 μm. The platelike BT/CT-x/y particles are polycrystals constructed from the nanocrystals (Fig. 2). The mean particle size of the nanocrystal in the samples of BT/CT-1/3, BT/CT-1/1, BT/CT-2/1, and BT/CT-6/1 is 241.02, 194.44, 109.05, and 101.78 nm, respectively (see Fig. S3(a^S–d^S)†). It is noticed that the individual nanocrystal is up to approx. 650 nm (in Fig. 2a and S3(a^S)†), which is not a thickness of the primary units. The constructed primary BT or CT units showing a scalelike morphology stack each other (Fig. 2). The thickness of the scalelike units is no more than 100 nm because the mean thickness is approximate 210 nm and the multiple layers of the primary crystalline units stack one on another. The size of the nanocrystals in the platelike particles decreases with the decrease of the content of CT. The result reveals that the crystallinity of the CT in the BT/CT-x/y samples decreases with the decrease of the content of CT, due to that the content of unreacted HT phase decreases with the increase of the BT content.

Nanostructures of samples. To further understand the nanostructures of the BT/CT-x/y samples obtained by the two-step solvothermal soft chemical process in detail, TEM/HRTEM observations and SAED investigations were performed, the results are illustrated in Fig. 3. All the TEM images present polycrystals with the platelike morphology and consistent with the SEM/FESEM results (Fig. 2 and S3 in the ESI†). It is very interesting that two sets of single-crystal-like diffraction spots can be simultaneously observed in each SAED pattern (Fig. 3b, e, h and k) of the polycrystalline samples. One can be attributed to the BT phase, and the other can be assigned to the CT phase, which are consistent with the XRD results (Fig. 1a–d). The (001) and (1−10) diffraction spots of BT and the (0−20) and (200) diffraction spots of CT were observed, respectively. The result reveals that the directions of the [001] and [1−10] of BT correspond to the directions of the [0−10] and [100] of CT,

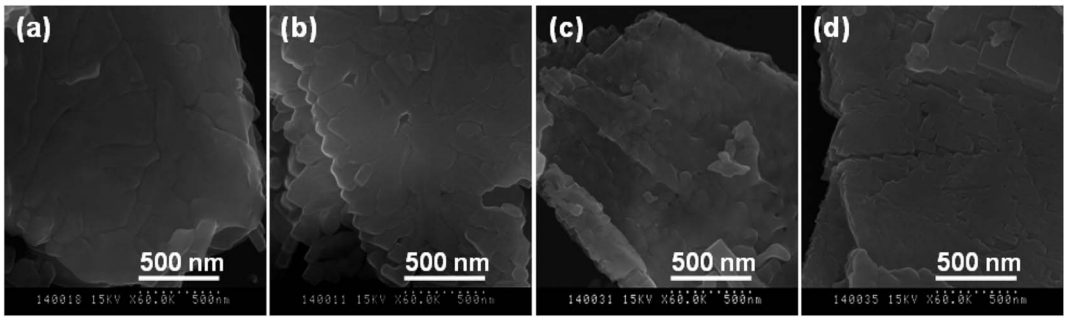

Fig. 2 FESEM images of samples of (a) BT/CT-1/3, (b) BT/CT-1/1, (c) BT/CT-2/1, and (d) BT/CT-6/1 obtained by solvothermal treatments of different BT/HT nanocomposites and $Ca(OH)_2$ in water–ethanol mixed solvent with volume ratio of 5 : 25 at 200 °C for 12 h, respectively.

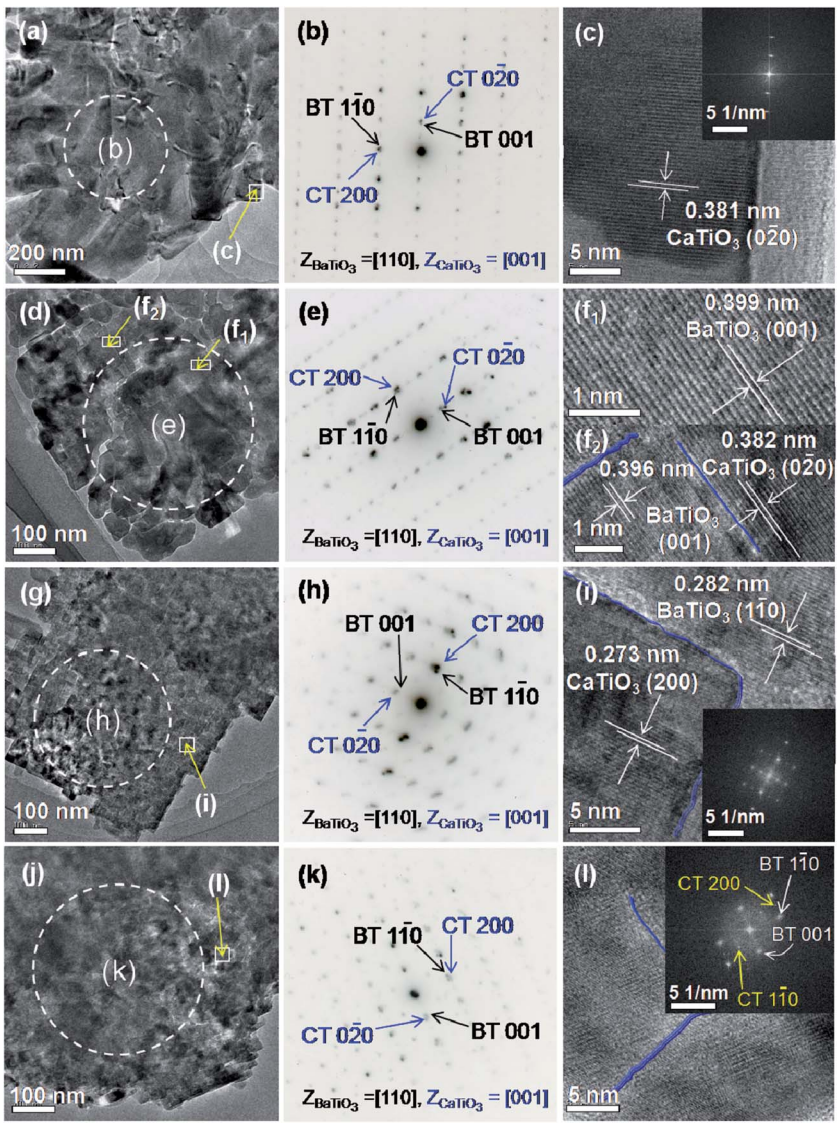

Fig. 3 (a, d, g and j) TEM images, (b, e, h and k) SAED patterns, and (c, f, i and l) HRTEM images of (a, b and c) BT/CT-1/3, (d, e and f) BT/CT-1/1, (g, h and i) BT/CT-2/1, and (j, k and l) BT/CT-6/1 samples obtained by solvothermal treatments of different BT/HT nanocomposites and $Ca(OH)_2$ in water–ethanol mixed solvent with volume ratio of 5 : 25 at 200 °C for 12 h, respectively. (c, f, i and l) HRTEM images derived from the (c, f, i and l) white panes in (a, d, g and j) TEM images, respectively. The inserted FFT (Fast Fourier Transformation) patterns derived from whole region of the corresponding HRTEM images, respectively. The blue lines in HRTEM images indicate the boundary regions between two primary nanocrystals.

respectively. These results suggest that the polycrystalline samples are constructed from the oriented BT and CT nanocrystals, where the [110] direction for all BT nanocrystals and the [001] direction for all CT nanocrystals are vertical to the basal plane of the platelike particle, respectively, in each platelike particle. Namely, the obtained polycrystalline platelike particles are mesocrystalline BT/CT nanocomposites. The formation of mesocrystalline BT/CT nanocomposites reveals *in situ* topochemical mesocrystal conversion mechanisms in the two-step solvothermal soft chemical process.[22]

In the HRTEM images (Fig. 3c, f, i and j), the lattice fringes of 0.396–0.399 nm (Fig. 3f_1 and f_2) and 0.282 nm (Fig. 3i) correspond to the (001) and (1−10) plane of the BT phase, respectively. The directions of the planes are consistent with the results in Fig. 3e and h, respectively. The lattice fringes of 0.381–0.382 nm (Fig. 3c and f_2) and 0.273 (Fig. 3i) nm correspond to the (0−20) and (200) plane of the CT phase, respectively. The directions of the planes are consistent with the results in Fig. 3b, e and h as well, respectively. The lattice fringes of the (001) and (1−10) plane of the BT phase are obviously close to the (0−20) and (200) plane of the CT phase, respectively, which can provide an evidence for the formation of the BT/CT heteroepitaxial interface in the nanocomposites. Such close lattice fringes can easily form the lattice strain. Their FFT patterns (inserted in Fig. 3c, i and l) agree with the corresponding SAED patterns in Fig. 3b, h and k, respectively. The crystal boundary regions indicated by the blue lines between BT and CT primary nanocrystals in a mesocrystal can be observed directly in the HRTEM images (Fig. 3f_2, i and l). These results described above reveal the obtained BT/CT hybrids are 2D crystal-axis-oriented nanocomposites. The nanocomposites are polycrystals constructed from well-aligned BT and CT nanocrystals. A confirmable topological relations between the BT and CT in the nanocomposites. The directions of the [001], [1−10] and [110] of crystalline BT correspond to the directions of the [0−10], [100], and [001] of crystalline CT, respectively. Such nanocomposites are 2D mesocrystalline nanocomposites with a high-density heteroepitaxial nanostructure.

Chemical compositions of mesocrystals. The chemical composition distributions in these 2D mesocrystalline BT/CT nanocomposites were investigated using EDS analysis. Fig. 4A shows representative EDS spectra of these nanocomposites. The mole ratios of Ti/Ba/Ca from the EDS analysis results in corresponding BT/CT nanocomposites are listed in Table S1 (see the ESI†). The average mole ratio results indicate that the Ca content decreases, while Ba content increases with the increase of the feed content of the BT. The sample of BT/CT-1/1 includes almost same fractions of the BT and CT phases. The corresponding EDS-mapping TEM images are shown in Fig. 4B and S5 (see (3) compositional analysis in the ESI†), respectively. In the EDS-mapping TEM images, the Ba and Ca elements are uniformly distributed on each 2D polycrystalline BT/CT-*x*/*y* particle, which implies that these 2D polycrystals are constructed from multiple layers of the primary crystalline BT and

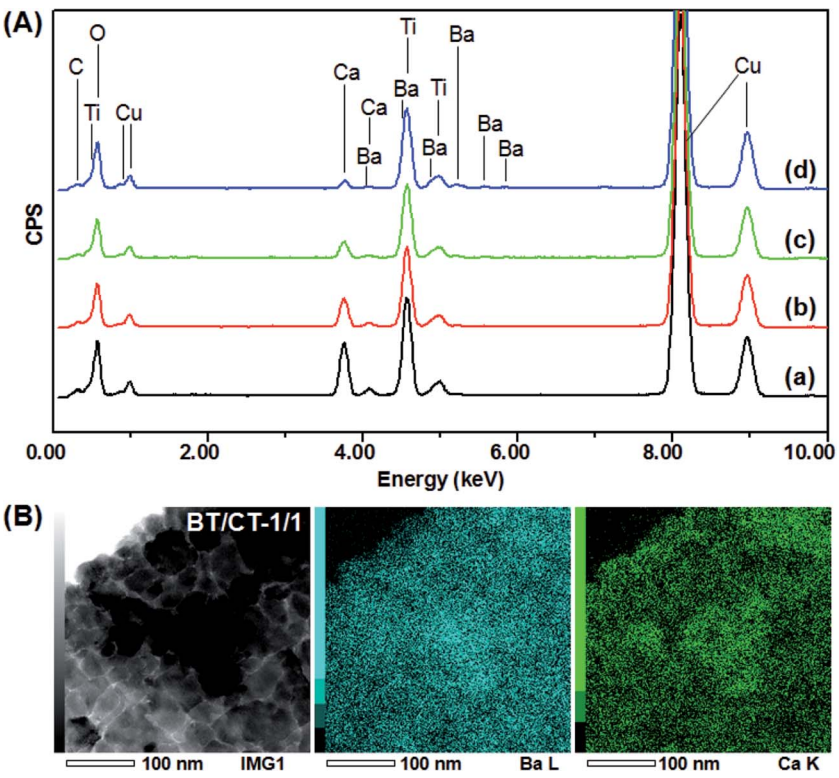

Fig. 4 (A) EDS spectra of (a) BT/CT-1/3, (b) BT/CT-1/1, (c) BT/CT-2/1, and (d) BT/CT-6/1 samples obtained by solvothermal treatments of different BT/HT nanocomposites and $Ca(OH)_2$ in water–ethanol mixed solvent with volume ratio of 5 : 25 at 200 °C for 12 h, respectively. (B) EDS-mapping TEM images of BT/CT-1/1 sample.

CT units stacked one on another. Nonetheless, a relationship between stacked primary crystalline BT and CT units of the inside of 2D polycrystals can be determined also from Fig. 3 results because the same topological relationship exists in the inside and surface of such mesocrystalline nanocomposite. This result is in accord with the mesocrystalline BT/ST nanocomposites derived from the 2D layered HT precursor.[23] For the BT/CT-1/1 sample, the concentration of the element Ba is similar to element Ca (see Fig. 4B). However, for the BT/CT-1/3 sample, the mapping color of the element Ca is strong and the element Ba is puny (see Fig. S5a†). The differences of the Ba and Ca contents in each mesocrystalline BT/ST nanocomposites can be made out *via* the concentration of the element mapping colors. This result agrees with the EDS spectra (see Fig. 4A). The Ba content increases and Ca content decreases, respectively, with the increase of the content of BT in the reaction system. These results are consistent with the EDS analysis results (Fig. 4A and Table S1 in the ESI†) and the XRD results (Fig. 1a–d). These results imply that the ratio of BT/CT can be adjusted by controlling the feed content of BT in the reaction system. Therefore, the density of the heteroepitaxial interface can be adjusted also in this manner. When the BT content is close to CT in the BT/CT nanocomposite, the highest density of the heteroepitaxial interface can be achieved.

Formation mechanism of the mesocrystalline BT/CT nanocomposite

Based on the description above and the results (Fig. 1–4) in the original text, a schematic representation of an *in situ* topochemical mesocrystal conversion mechanism from the layered HT single crystal precursor to the mesocrystalline BT/CT nanocomposite can be illustrated in Fig. 5. Before reaction, in the crystal structure of the layered HT lepidocrocite, the host sheets are stacked with a basal spacing of about 0.882 nm in a body-centered orthorhombic system, accommodating H_2O and H_3O^+ between them.[24] In the first step, the partial HT crystal is transformed into BT nanocrystals because the Ti/Ba mole ratio in the reaction system is less than 1. Initially, Ba^{2+} are intercalated into the HT bulk crystal through its interlayer pathway by an H^+/Ba^{2+} exchange reaction, and then the Ba^{2+} react with the TiO_6 octahedral layers of HT in the bulk crystal to form the BT phase.[19] Therefore, the 2D BT/HT nanocomposites formed by this reaction have uniform distributions of BT nanoparticles in the bulk crystals. In the present case, the topochemical conversion reaction is dominant in the water solvent, owing to the low concentration of $Ba(OH)_2$.[18,22] In the second step of the solvothermal treatment of the BT/HT nanocomposite in the $Ca(OH)_2$ suspensions, another topochemical conversion reaction occurs similar to the first step. In this step, incipiently, the Ca^{2+} are intercalated into the residual HT matrix crystal through the interlayer pathway by an H^+/Ca^{2+} exchange reaction, and then the Ca^{2+} react with the unreacted HT matrix crystal to form the CT nanocrystals until consuming all the HT phase. Because the generated BT nanocrystals are well-aligned and show the same direction orientation,[23] the CT nanocrystals generated against the BT nanocrystals and grew by a heteroepitaxial growth process, resulting in the topochemical formation of the crystal-axis-oriented mesocrystalline BT/CT nanocomposite with heteroepitaxial nanostructure, which is different from the formation mechanism of oriented attachment.[28] There is a definite crystallographic topological relationship between the crystal-axis directions of the oriented BT and CT nanocrystals (see Fig. 5) existing in the mesocrystalline BT/CT nanocomposite homogeneously. The directions of the [001], [110], and [1−10] of BT correspond to the directions of the [0−20], [001], and [200] of CT, respectively (see Fig. 5). In addition, the chemical composition distributions in these 2D mesocrystalline BT/CT nanocomposites are uniform. Therefore, such 2D mesocrystalline BT/CT nanocomposites own stacking nanostructure and high-density heteroepitaxial interface.

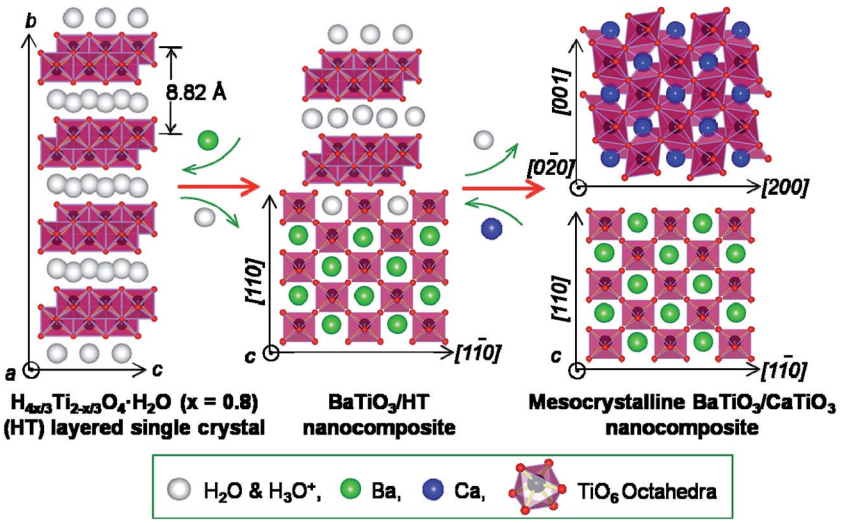

Fig. 5 Schematic representation of crystallographic variation of crystalline structure from layered HT single crystal to mesocrystalline $BaTiO_3/CaTiO_3$ nanocomposite *via in situ* topochemical mesocrystalline conversion reaction.

Piezoelectric responses of the mesocrystals

The piezoelectric responses of the individual platelike particles of the mesocrystalline BT/CT nanocomposites were recorded by a scanning probe microscopy (SPM) system. Fig. 6a and S6 (see (4) piezoelectric response in the ESI†) illustrate the typical butterfly loops of electric-field-induced displacements for individual mesocrystals obtained by the two-step solvothermal soft chemical process, and the converse piezoelectric coefficients were also calculated and labeled to the right axis. The long-term piezoelectric responses can be confirmed by the PRM systems though the examination is exposed to a higher number of applied voltage cycles. The performance test is repeated for 6 times, showing good repetitiveness. The d^*_{33} value in this study is an average value. The BT/CT-x/y nanocomposites show a higher piezoelectric response than the pure CT mesocrystals and BT mesocrystals (Fig. 6b). A significantly high converse piezoelectric response with an average d^*_{33} up to ~208 pm V^{-1} is observed for BT/CT-1/1 nanocomposite, as shown in Fig. 6, which is the highest in the titanate mesocrystal samples studied here (Fig. 6b and S6 in the ESI†). The highest d^*_{33} value for the BT/CT-1/1 nanocomposite is higher than those of BT (35 pm V^{-1}) and CT (40.9 pm V^{-1}) mesocrystals by more than five times, and also higher than the reported $BaTiO_3$ (28 pm V^{-1}),[29] $NaNbO_3$ (4.26 pm V^{-1}),[30] and (K, Na) NbO_3 (113 pm V^{-1})[31] perovskite nano-individuals. This value is similar to the 1D (K, Na) NbO_3 (230 pm V^{-1}) large nanorod[26] and ($Bi_{0.5}Na_{0.5}$) TiO_3 nanofibre (~18 pm V^{-1})[32] with single crystalline nature. These results reveal that the BT/CT-x/y nanocomposites own a higher piezoelectric response than a single crystalline nature, suggesting the heteroepitaxial interface in the nanocomposites plays a critical role for the enhancement of the piezoelectric property.

The BT/CT-1/1 nanocomposite exhibits the specific advantage on the piezoelectric responses, which is higher than that of mesocrystalline BT/ST nanocomposites before annealing treatment.[23] It may be owing to the difference of the incipient ferroelectric orthorhombic CT and the quantum paraelectric cubic ST.[33] The piezoelectric results suggest that the BT/CT nanocomposites can achieve a high piezoelectric response due to the lattice strain at BT/CT heteroepitaxial interface. The highest piezoelectric response of BT/CT-1/1 with the composition close to BT/CT = 1/1 is due to the lattice strain derived from its heteroepitaxial interfaces with the highest density in the nanocomposite.

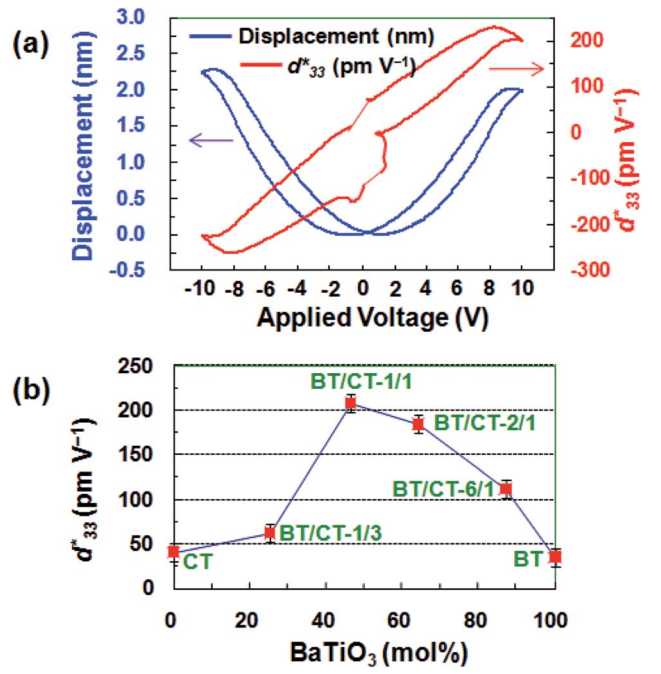

Fig. 6 (a) Displacement–voltage curve and calculated converse piezoelectric coefficient curve of mesocrystalline BT/CT mesocrystal (BT/CT-1/1) obtained by solvothermal treatment of BT/HT nanocomposite and $Ca(OH)_2$ in water–ethanol mixed solvent. (b) Variations of converse piezoelectric coefficients (d^*_{33}) of mesocrystalline BT/CT nanocomposites with different compositions, CT mesocrystals, and BT mesocrystals.

4 Conclusions

The novel 2D nanocrystal-aligned mesocrystalline BT/CT nanocomposites with controllable compositions were successfully synthesized by using a two-step solvothermal soft chemical process for the first time. These nanocomposites are polycrystals constructed from well-aligned BT and CT nanocrystals. There is a definite crystallographic topological relationship between the crystal-axis directions of the oriented BT and CT nanocrystals. All BT and CT nanocrystals in a platelike BT/CT nanocomposite particle show the same direction orientation, respectively, which gives two sets of single-crystal-like electron diffraction spots patterns. The mesocrystalline nanocomposites were formed *via* an *in situ* topochemical mesocrystal conversion mechanism. The BT/CT nanocomposite shows an average piezoelectric coefficient d^*_{33} of 208 pm V^{-1} which is five times larger than that of BT mesocrystal. The BT/CT nanocomposites have high-density BT/CT heteroepitaxial nanostructure which exhibits the specific enhancement of piezoelectric response due to introduction of lattice strain at the interface.

Conflict of interest

The authors declare no competing financial interest.

Acknowledgements

This work was supported in part by Grants-in-Aid for Scientific Research (B) (No. 26289240) from Japan Society for the Promotion of Science. This work was also supported in part by the National Natural Science Foundations of China (No. 21005003, No. 21501007, and No. 1502163), the Industrial Science and Technology Plan in Shaanxi Province of China (No. 2016GY-229), the Natural Science Foundation of Shaanxi Provincial Department of Education (16JF001), the Doctoral Scientific Research Starting Foundation of Baoji University of Arts and Science (No. ZK15050), and the Scientific and technological research and Development Plan in Baoji City of China (No. 15RKX-1-5-1).

Notes and references

1 H. N. Lee, H. M. Christen, M. F. Chisholm, C. M. Rouleau and D. H. Lowndes, *Nature*, 2005, **433**, 395–399.
2 J. C. Agar, R. V. K. Mangalam, A. R. Damodaran, G. Velarde, J. Karthik, M. B. Okatan, Z. H. Chen, S. Jesse, N. Balke, S. V. Kalinin and L. W. Martin, *Adv. Mater. Interfaces*, 2014, **1**, 1400098.
3 J. Zhang, Z. L. Yang, F. Z. Lv, C. X. Gao and D. S. Xue, *RSC Adv.*, 2014, **4**, 61046–61050.
4 W. Sun, Q. Yu, J. Y. Li and J.-F. Li, *J. Phys. Chem. C*, 2015, **119**, 19891–19896.
5 P. Zerrer, H. Wang, H. Yang, J. Yoon, A. Fouchet, R. Yu, M. G. Blamire and Q. X. Jia, *Nat. Mater.*, 2008, **7**, 314–320.
6 S. A. Harrington, J. Zhai, S. Denev, V. Gopalan, H. Wang and Z. Bi, *Nat. Nanotechnol.*, 2011, **6**, 491–495.
7 E. Benckiser, M. W. Haverkort, S. Brück, E. Goering, S. Macke, A. Frañó, X. Yang, O. K. Andersen, G. Cristiani, H. U. Habermeier, A. V. Boris, I. Zegkinoglou, P. Wochner, H. J. Kim, V. Hinkov and B. Keimer, *Nat. Mater.*, 2011, **10**, 189–193.
8 Y. Zhang, C. H. Liu, J. B. Liu, J. Xiong, J. Y. Liu, K. Zhang, Y. D. Liu, M. Z. Peng, A. F. Yu, A. H. Zhang, Y. Zhang, Z. W. Wang, J. Y. Zhai and Z. L. Wang, *ACS Appl. Mater. Interfaces*, 2016, **8**, 1381–1387.
9 K. Kathan-Galipeau, P. P. Wu, Y. L. Li, L.-Q. Chen, A. Soukiassian, X. X. Xi, D. G. Schlom and D. A. Bonnell, *ACS Nano*, 2011, **5**, 640–646.
10 A. P. Levanyuk and I. B. Misirlioglu, *Appl. Phys. Lett.*, 2013, **103**, 192906.
11 N. Suzuki, M. B. Zakaria, N. L. Torad, K. C.-W. Wu, Y. Nemoto, M. Imura, M. Osada and Y. Yamauchi, *Chem.–Eur. J.*, 2013, **19**, 4446–4450.
12 D. Kar and D. Das, *RSC Adv.*, 2015, **5**, 61118–61126.
13 H. Cölfen and M. Antonietti, *Angew. Chem., Int. Ed.*, 2005, **44**, 5576–5591.
14 V. Kalyani, B. S. Vasile, A. Ianculescu, M. T. Buscaglia, V. Buscaglia and P. NanniCryst, *Cryst. Growth Des.*, 2012, **12**, 4450–4456.
15 D. V. Talapin, J.-S. Lee, M. V. Kovalenko and E. V. Shevchenko, *Chem. Rev.*, 2010, **110**, 389–458.
16 T. H. Han, H. G. Wang and X. M. Zheng, *RSC Adv.*, 2016, **6**, 7829–7837.
17 R. Q. Song and H. Cölfen, *Adv. Mater.*, 2010, **12**, 1301–1330.
18 Q. Feng, M. Hirasawa and K. Yanagisawa, *Chem. Mater.*, 2001, **13**, 290–296.
19 X. G. Kong, D. W. Hu, Y. Ishikawa, Y. Tanaka and Q. Feng, *Chem. Mater.*, 2011, **23**, 3978–3986.
20 X. G. Kong, Y. Ishikawa, K. Shinagawa and Q. Feng, *J. Am. Ceram. Soc.*, 2011, **94**, 3716–3721.
21 D. W. Hu, X. G. Kong, K. Mori, Y. Tanaka, K. Shinagawa and Q. Feng, *Inorg. Chem.*, 2013, **52**, 10542–10551.
22 D. W. Hu, X. Luo, X. G. Kong, Y. Wang, Y. Tanaka and Q. Feng, *CrystEngComm*, 2015, **17**, 1758–1764.
23 D. W. Hu, H. Ma, Y. Tanaka, L. F. Zhao and Q. Feng, *Chem. Mater.*, 2015, **27**, 4983–4994.
24 D. W. Hu, W. X. Zhang, Y. Tanaka, N. Kusunose, Y. G. Peng and Q. Feng, *Cryst. Growth Des.*, 2015, **15**, 1214–1225.
25 J. V. Lauritsen, S. Porsgaard, M. K. Rasmussen, M. C. R. Jensen, R. Bechstein, K. Meinander, B. S. Clausen, S. Helveg, R. Wahl and G. Kresse, *ACS Nano*, 2011, **7**, 5987–5994.
26 L.-Q. Cheng, K. Wang and J.-F. Li, *Chem. Commun.*, 2013, **49**, 4003–4005.
27 P. Pinceloup, C. Courtois, A. Leriche and B. Thierry, *J. Am. Ceram. Soc.*, 1999, **82**, 3049–3056.
28 K. Yasui and K. Kato, *J. Phys. Chem. C*, 2015, **119**, 24597–24605.
29 Z. Deng, Y. Dai, W. Chen, X. M. Pei and J. H. Liao, *Nanoscale Res. Lett.*, 2010, **5**, 1217–1221.
30 T. Y. Ke, H. A. Chen, H. S. Sheu, J. W. Yeh, H. N. Lin, C. Y. Lee and H. T. Chiu, *J. Phys. Chem. C*, 2008, **112**, 8827–8831.
31 S. Y. Xu and J.-F. Li, *J. Am. Ceram. Soc.*, 2011, **94**, 3812–3818.
32 M. B. Ghasemian, Q. R. Lin, E. Adabifiroozjaei, F. F. Wang, D. W. Chu and D. Y. Wang, *RSC Adv.*, 2017, **7**, 15020–15026.
33 W. Kinasea and K. Harad, *Ferroelectrics*, 2003, **283**, 39–47.